The American Journal of Human Genetics, Volume *108*

Supplemental information

Altered replication stress response due to *CARD14* mutations promotes recombination-induced revertant mosaicism

Toshinari Miyauchi, Shotaro Suzuki, Masae Takeda, Jin Teng Peh, Masayuki Aiba, Ken Natsuga, Yasuyuki Fujita, Takuya Takeichi, Taiko Sakamoto, Masashi Akiyama, Hiroshi Shimizu, and Toshifumi Nomura

Figure S1

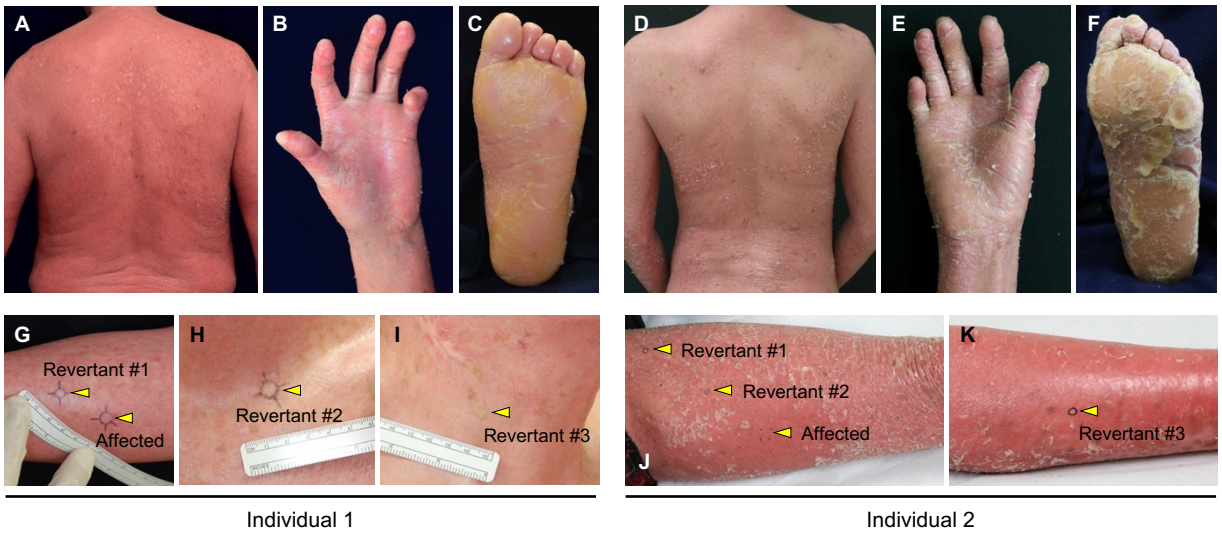
A
B
C
D
E
F
G
Revertant #1
Affected
H
Revertant #2
I
Revertant #3
Revertant #1
Revertant #2
Affected
J
K
Revertant #3
Individual 1
Individual 2

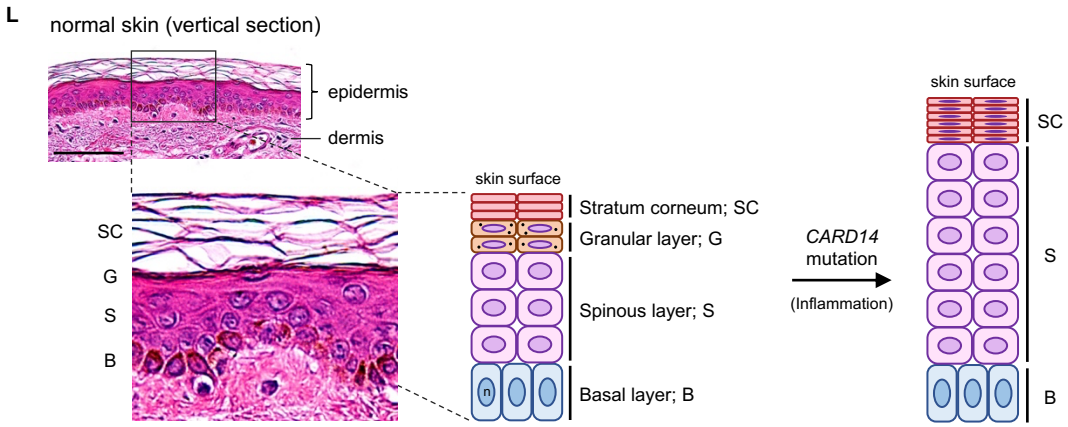
L
normal skin (vertical section)
epidermis
dermis
SC
G
S
B
skin surface
Stratum corneum; SC
Granular layer; G
Spinous layer; S
Basal layer; B
CARD14 mutation
(Inflammation)
skin surface
SC
S
B


M
Affected skin
Revertant spot #2
Revertant spot #3

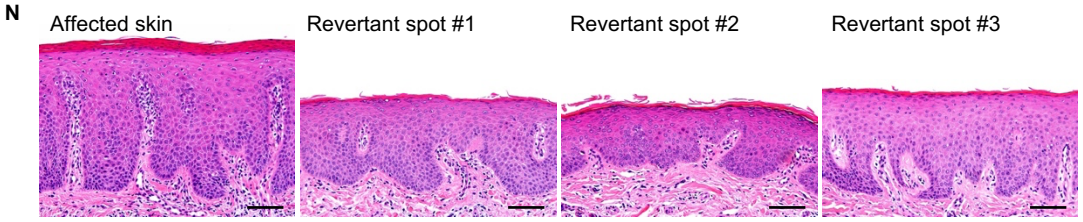
N
Affected skin
Revertant spot #1
Revertant spot #2
Revertant spot #3

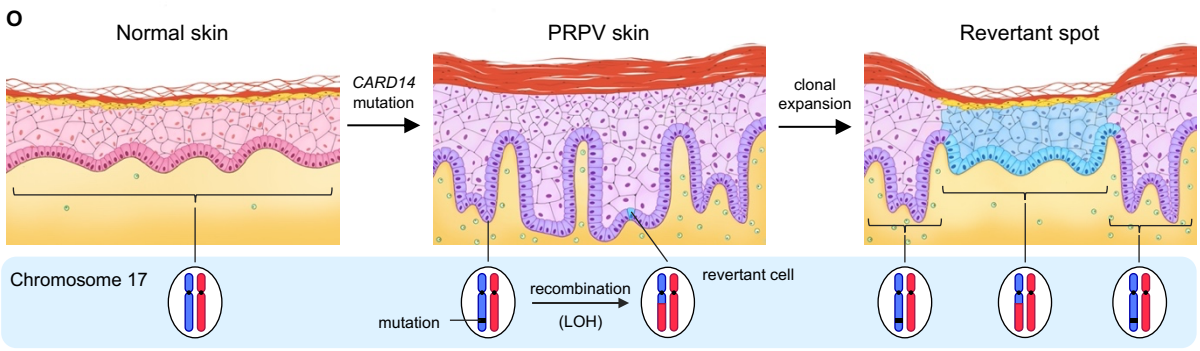
O
Normal skin
CARD14 mutation
PRPV skin
clonal expansion
Revertant spot
Chromosome 17
mutation
recombination
(LOH)
revertant cell

Figure S1. Clinical and histological features of individual 1 and 2

(A-C) Generalized scaly erythema (A) and palmoplantar keratoderma (B and C) were observed in individual 1. Joint contractures of the fingers were also noted (B). Although the patient was originally diagnosed as having congenital ichthyosiform erythroderma at the timing of previous publications, we performed whole-exome sequencing in this study, which led to identification of a pathogenic *CARD14* mutation. In contrast, no pathogenic variants were identified in any of the known causative genes for non-syndromic ichthyoses, including congenital ichthyosiform erythroderma (See Table S1). Based on these findings, we ultimately diagnosed the patient as having PRPV.

(D-F) Individual 2 exhibited skin symptoms similar to individual 1.

(G-K) Both patients showed multiple normal-appearing spots. Skin biopsy was taken from the left forearm (G), left anterior chest (H), and right neck (I) of individual 1 and from the left thigh (J) and left lower leg (K) of individual 2.

(L) Normal skin structure and structural changes due to *CARD14* mutations. The epidermis (the outermost layer of the skin) is composed of layers of epithelial cells (keratinocytes). Beneath the epidermis lies the dermis comprising connective tissues and housing various appendages including blood vessels, hair follicles, sweat glands, and other structures. The normal epidermis has four layers: basal layer (B), spinous layer (S), granular layer (G), and stratum corneum (SC). Proliferative epidermal progenitors reside in basal layer, and all the cells above this layer are differentiated cells. Histology of the skin with *CARD14* mutations shows epidermal thickening (acanthosis), lack of a granular layer, and thickening of stratum corneum (hyperkeratosis) with retained nuclei (parakeratosis).

(M and N) Histological comparison between affected skin and revertant spots of individual 1 (M) and individual 2 (N). Hematoxylin and eosin staining. Scale bars, 100 μm.

(O) Schematic comparison among normal skin, PRPV skin, and revertant spot. The birth of a revertant cell via mitotic recombination and its clonal expansion leads to the appearance of clinically visible revertant spot.

Figure S2

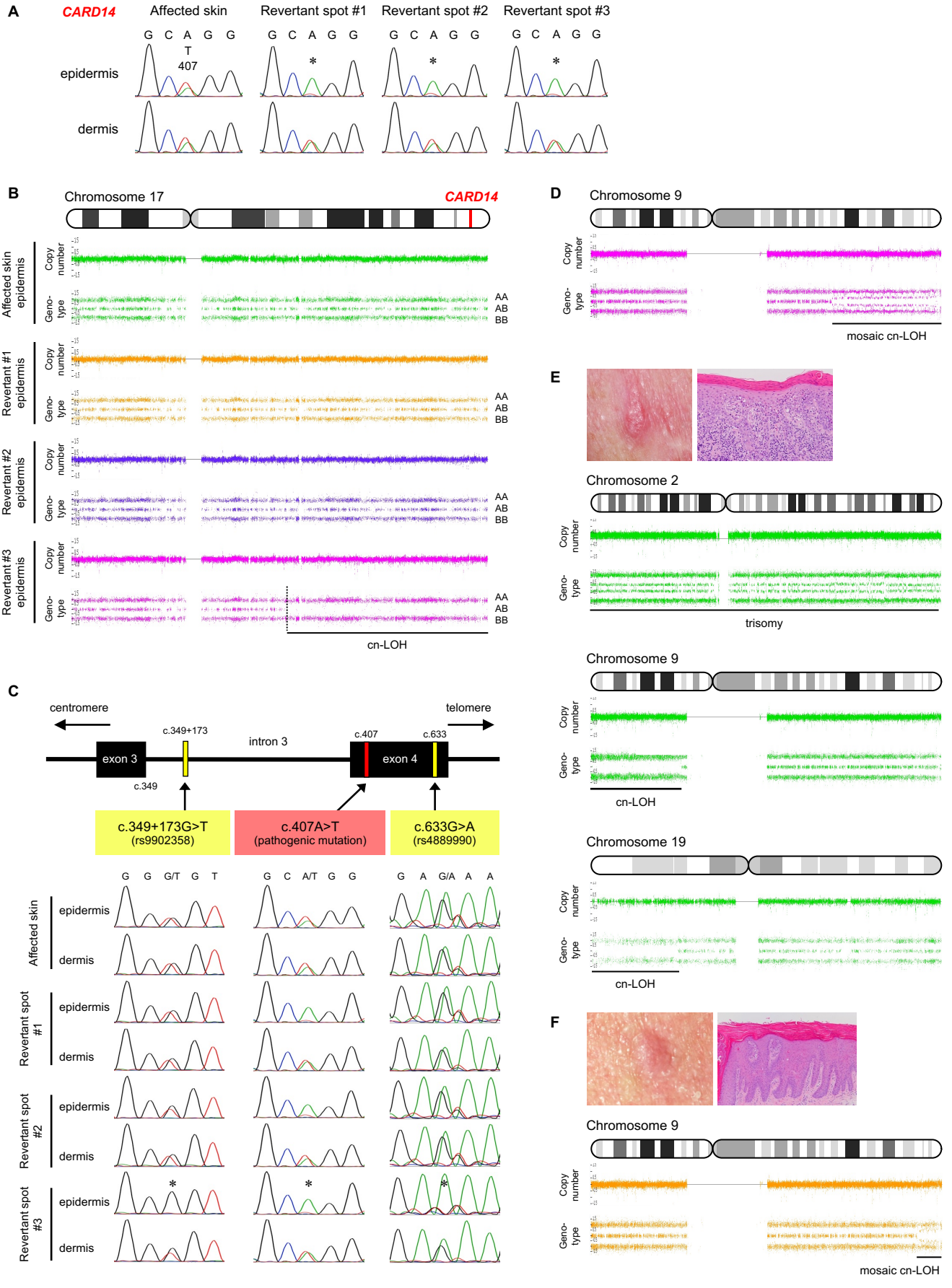
A
CARD14
Affected skin
Revertant spot #1
Revertant spot #2
Revertant spot #3
G C A G G
T
407
epidermis
dermis
B
Chromosome 17
CARD14
Affected skin epidermis
Revertant #1 epidermis
Revertant #2 epidermis
Revertant #3 epidermis
Copy number
Geno-type
AA
AB
BB
cn-LOH
C
centromere
telomere
c.349+173
intron 3
c.407
c.633
exon 3
exon 4
c.349
c.349+173G>T
(rs9902358)
c.407A>T
(pathogenic mutation)
c.633G>A
(rs4889990)
G G G/T G T
G C A/T G G
G A G/A A A
epidermis
dermis
Affected skin
Revertant spot #1
Revertant spot #2
Revertant spot #3
D
Chromosome 9
mosaic cn-LOH
E
Chromosome 2
trisomy
Chromosome 9
cn-LOH
Chromosome 19
cn-LOH
F
Chromosome 9
mosaic cn-LOH

Figure S2. Genetic features of individual 1 and 2

(A) Mutation analysis of *CARD14* using genomic DNA extracted from skin samples in individual 2. The heterozygous missense mutation, c.407A>T, is absent in the revertant epidermis (*).

(B) SNP array data of chromosome 17 from individual 2. LOH was identified in 1 of 3 revertant spots. Dotted lines represent the breakpoint of recombination.

(C) Heterozygous SNPs (c.349+173G>T and c.633G>A) on both sides closest to the pathogenic mutation in individual 2 were absent in the epidermis of revertant spot #3 (*) but were still present in the epidermis of revertant spots #1 and #2. Back mutation most likely explains the genetic reversion in revertant spots #1 and #2.

(D) Revertant spot #2 of individual 1 also harbors mosaic cn-LOH on chromosome 9.

(E and F) Clinical, pathological, and genetic features of SCC in situ arising on the left neck (E) and the posterior neck (F) of individual 1.

Figure S3

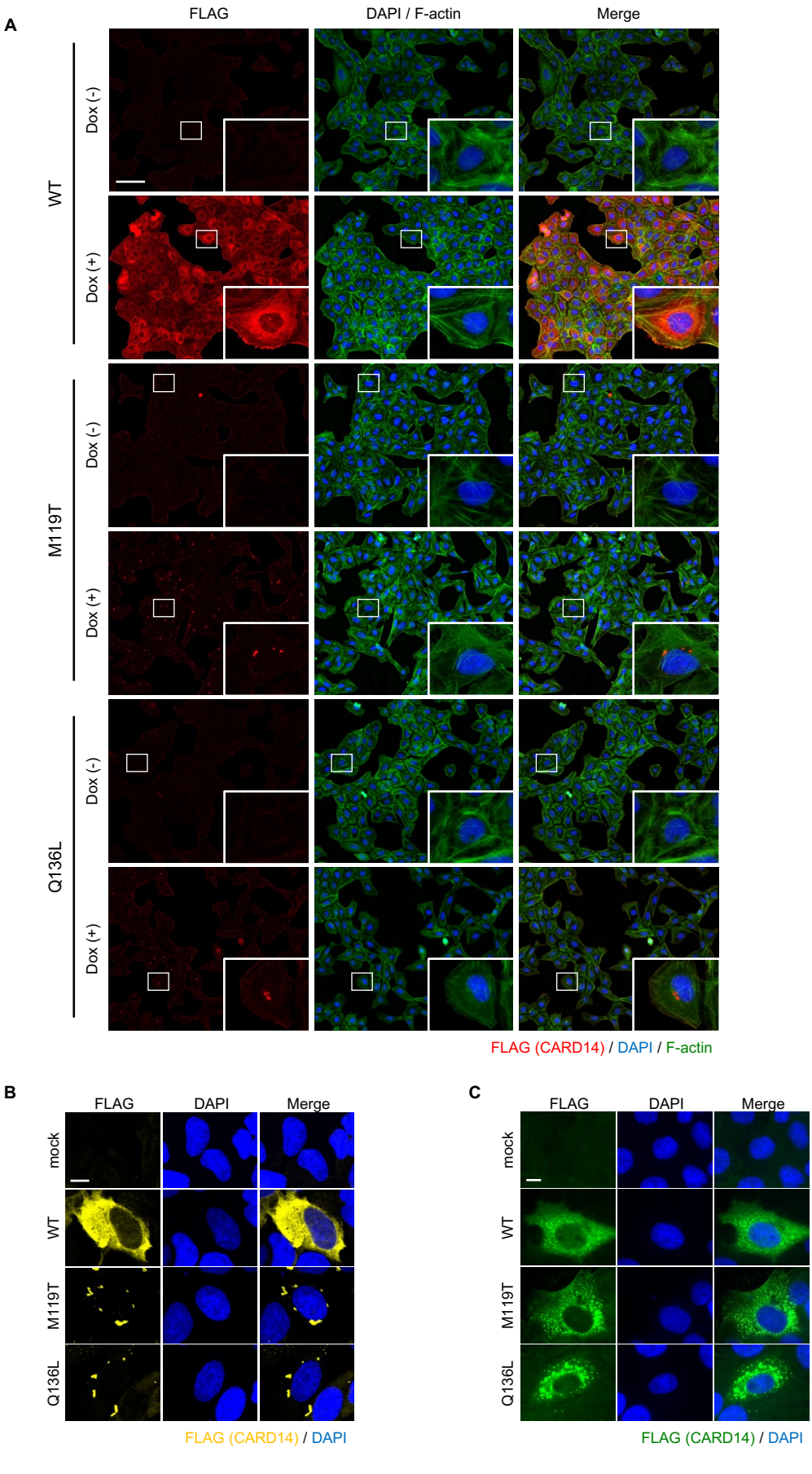
A
FLAG
DAPI / F-actin
Merge
WT
M119T
Q136L
Dox (-)
Dox (+)
FLAG (CARD14) / DAPI / F-actin
B
FLAG
DAPI
Merge
mock
WT
M119T
Q136L
FLAG (CARD14) / DAPI
C
FLAG
DAPI
Merge
mock
WT
M119T
Q136L
FLAG (CARD14) / DAPI

Figure S3. immunofluorescence microscopy revealing intracellular CARD14 localization

(A) Immunofluorescence of CARD14 cell lines incubated with or without Dox for 24 h. Insets represent a high magnification of the area indicated in the boxes. Scale bar, 100 μm. (B and C) Aberrant distribution of mut-CARD14 was further confirmed by transient overexpression analyses using U2OS cells (B) and HaCaT cells (C). Scale bar, 10 μm. WT, wild-type; M119T, p.Met119Thr; Q136L, p.Gln136Leu.

Figure S4

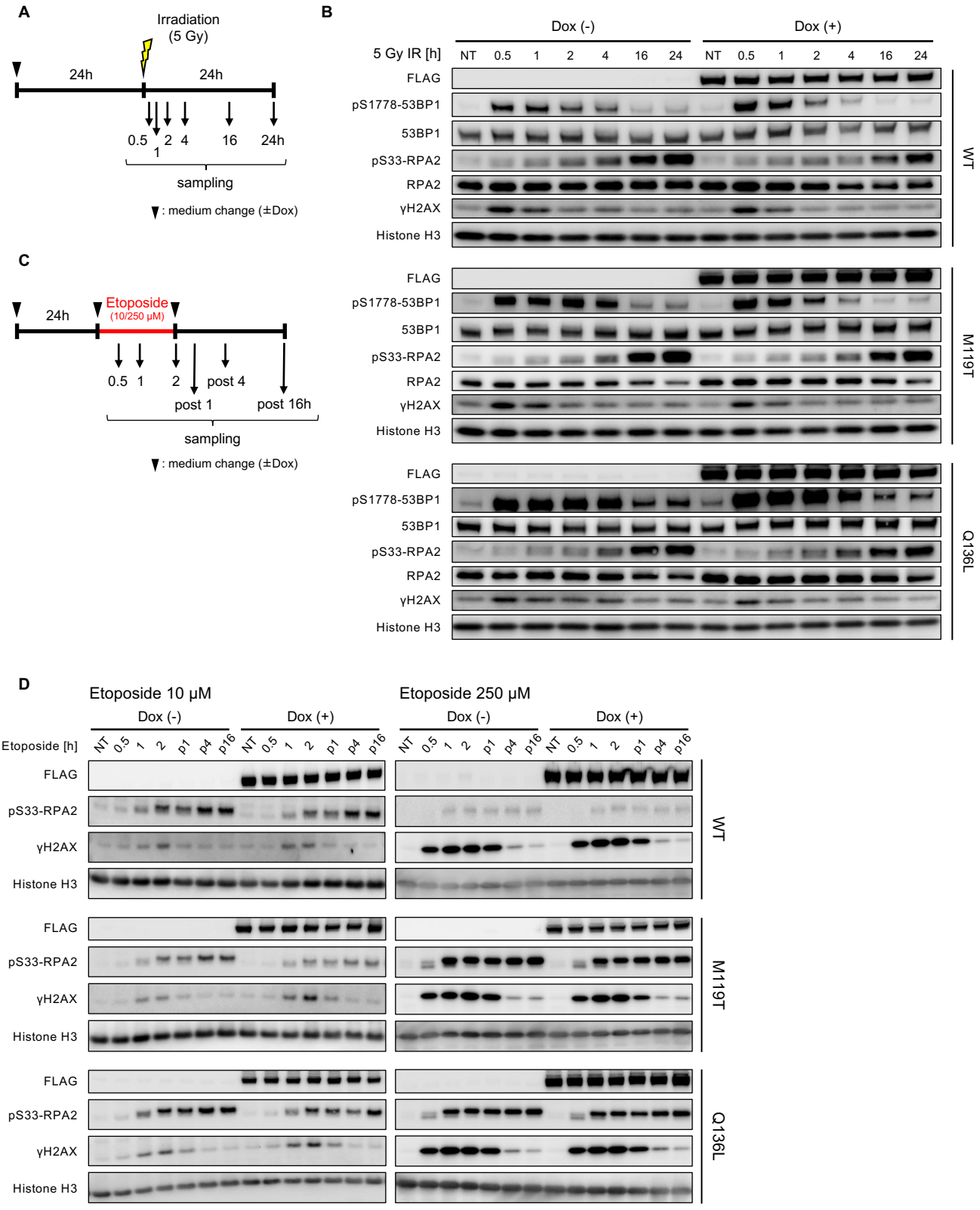
A
Irradiation
(5 Gy)
24h
24h
0.5
1
2
4
16
24h
sampling
▼: medium change (±Dox)
B
Dox (-)
Dox (+)
5 Gy IR [h]
NT 0.5 1 2 4 16 24 NT 0.5 1 2 4 16 24
FLAG
pS1778-53BP1
53BP1
pS33-RPA2
RPA2
γH2AX
Histone H3
WT
M119T
Q136L
C
24h
Etoposide
(10/250 μM)
0.5 1 2 post 4
post 1
post 16h
sampling
▼: medium change (±Dox)
D
Etoposide 10 μM
Etoposide 250 μM
Dox (-)
Dox (+)
Etoposide [h]
NT 0.5 1 2 p1 p4 p16
FLAG
pS33-RPA2
γH2AX
Histone H3
WT
M119T
Q136L

Figure S4. Mut-CARD14 expression provides no difference in the DNA damage response

(A) Schematic depicting timeline of when cells were exposed to 5 Gy IR. Whole-cell lysate was prepared at indicated times.

(B) Immunoblots showing the levels of DNA damage and the activation of 53BP1 and RPA2 following irradiation. pS1778-53BP1, phospho-Ser1778 53BP1. pS33-RPA2, phospho-Ser33 RPA2. NT, non-treatment.

(C) Schematic depicting timeline of when cells were exposed to 10 or 250 μM etoposide and when the samples were obtained.

(D) Whole-cell lysate was immunoblotted with the indicated antibodies. p1/4/16, post 1/4/16 h. NT, non-treatment; WT, wild-type; M119T, p.Met119Thr; Q136L, p.Gln136Leu.

Figure S5

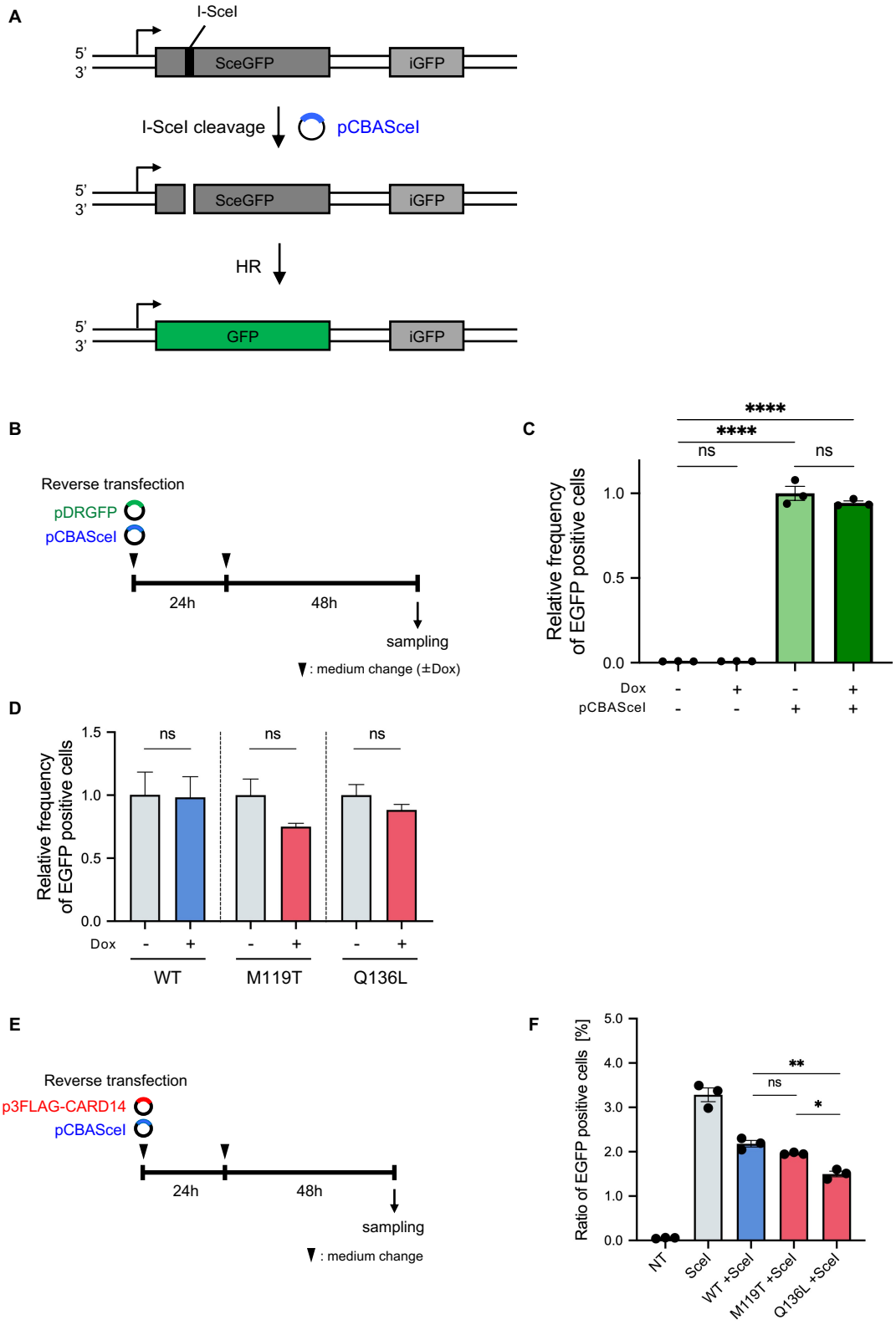
A
I-SceI
5'
3'
SceGFP
iGFP
I-SceI cleavage
pCBASceI
HR
GFP
B
Reverse transfection
pDRGFP
pCBASceI
24h
48h
sampling
: medium change (±Dox)
C
****
****
ns
ns
Relative frequency of EGFP positive cells
1.0
0.5
0.0
Dox
pCBASceI
D
ns
ns
ns
Relative frequency of EGFP positive cells
1.5
1.0
0.5
0.0
Dox
WT
M119T
Q136L
E
Reverse transfection
p3FLAG-CARD14
pCBASceI
24h
48h
sampling
: medium change
F
Ratio of EGFP positive cells [%]
5.0
4.0
3.0
2.0
1.0
0.0
**
ns
*
NT
SceI
WT +SceI
M119T +SceI
Q136L +SceI

Figure S5. Measurement of HR-mediated DSB repair frequency

(A) Schematic showing the process of EGFP expression in DR-GFP assay. *SceGFP* gene contains I-SceI endonuclease site and cellular I-SceI expression leads to a DSB at this site. The DSB can be repaired by HR using downstream wild-type GFP sequence (iGFP) as a template, resulting in EGFP expression.

(B and C) Schematic depicting timeline of DR-GFP assay and when transient transfection of the DR-GFP reporter (pDRGFP) and I-SceI (pCBASceI) vectors was used (B). EGFP positive cells did not appear when U2OS cells were transfected with only pDRGFP but appeared when transfected with both pDRGFP and pCBASceI (C). DR-GFP assay works well even in transient transfection system; n = 3 independent experiments; error bars represent SEM.

(D) DR-GFP assay by transient transfection revealed that neither wt-CARD14 nor mut-CARD14 increased HR frequency; n = 3 independent experiments. Error bars represent SEM

(E and F) Schematic of DR-GFP assay using U2OS cells stably expressing the DR-GFP reporter (E). In this assay, pCBASceI ± p3FLAG-CARD14 were transiently transfected (E). Again, neither wt-CARD14 nor mut-CARD14 promoted HR (F); n = 3 independent experiments; error bars represent SEM NT, non-treatment. Statistical significance was calculated using one-way ANOVA followed by a multiple comparisons test. *$P < 0.05$, **$P < 0.01$, ****$P < 0.0001$; ns, not significant. WT, wild-type; M119T, p.Met119Thr; Q136L, p.Gln136Leu.

Figure S6

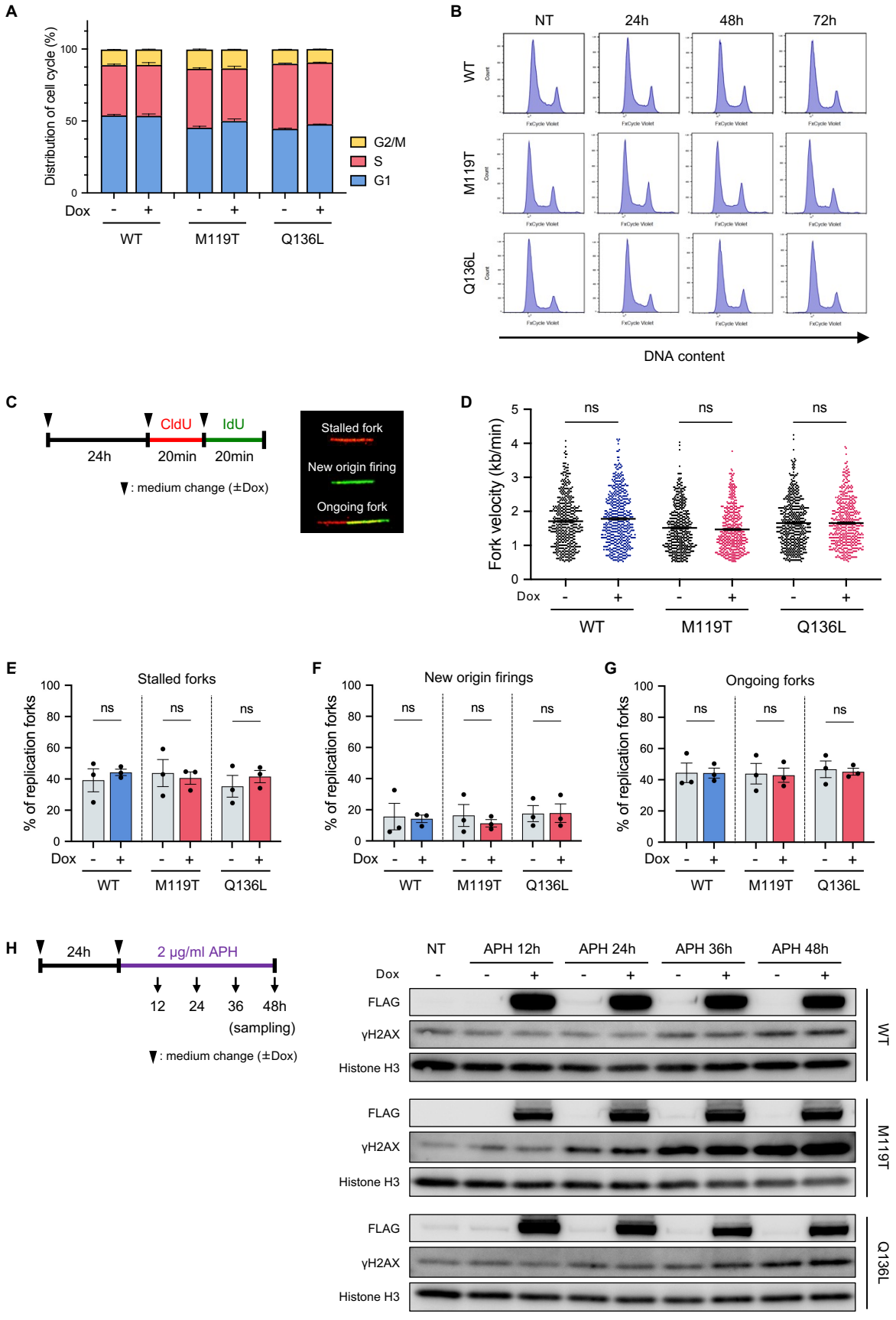
A
Distribution of cell cycle (%)
100
50
0
G2/M
S
G1
Dox - + - + - +
WT
M119T
Q136L
B
NT
24h
48h
72h
WT
M119T
Q136L
DNA content
C
CldU
IdU
24h
20min
20min
: medium change (±Dox)
Stalled fork
New origin firing
Ongoing fork
D
Fork velocity (kb/min)
ns
Dox - + - + - +
WT
M119T
Q136L
E
Stalled forks
% of replication forks
F
New origin firings
G
Ongoing forks
H
24h
2 μg/ml APH
12
24
36
48h
(sampling)
: medium change (±Dox)
NT
APH 12h
APH 24h
APH 36h
APH 48h
Dox
FLAG
γH2AX
Histone H3
WT
M119T
Q136L

Figure S6. Effect of Mut-CARD14 expression on dna replication

(A) Cell cycle profiles of CARD14 cell lines at 24 h following Dox addition. For each sample, 30,000 cells were analyzed; n = 3 independent experiments; Error bars represent SEM.

(B) Representative histograms of DNA content of CARD14 cell lines 24, 48, 72 h following Dox addition.

(C) Schematic depicting timeline of how cells are labeled with CldU and IdU. Representative images of a stalled fork, new origin firing, and ongoing fork are also shown.

(D) Comparison of replication fork velocity with or without Dox. At least 500 fibers for each cell line were quantified. Experiments were repeated at least thrice, and similar results were obtained each time. Horizontal lines represent mean values ± SEM. Statistical significance was calculated using the Mann-Whitney U test. ns, not significant.

(E-G) Quantification of the percentage of stalled forks (E), new origin firings (F), and ongoing forks (G) to all CldU-labeled forks; n = 3 independent experiments; error bars represent SEM. Statistical significance was calculated using the two-tailed *t*-test. ns, not significant.

(H) Schematic depicting timeline of when cells were treated with 2 μg/ml APH and when samples were obtained. Whole-cell lysate was immunoblotted with indicated antibodies. Prolonged APH treatment increased γH2AX in the presence of mut-CARD14. NT, non-treatment; WT, wild-type; M119T, p.Met119Thr; Q136L, p.Gln136Leu.

Figure S7

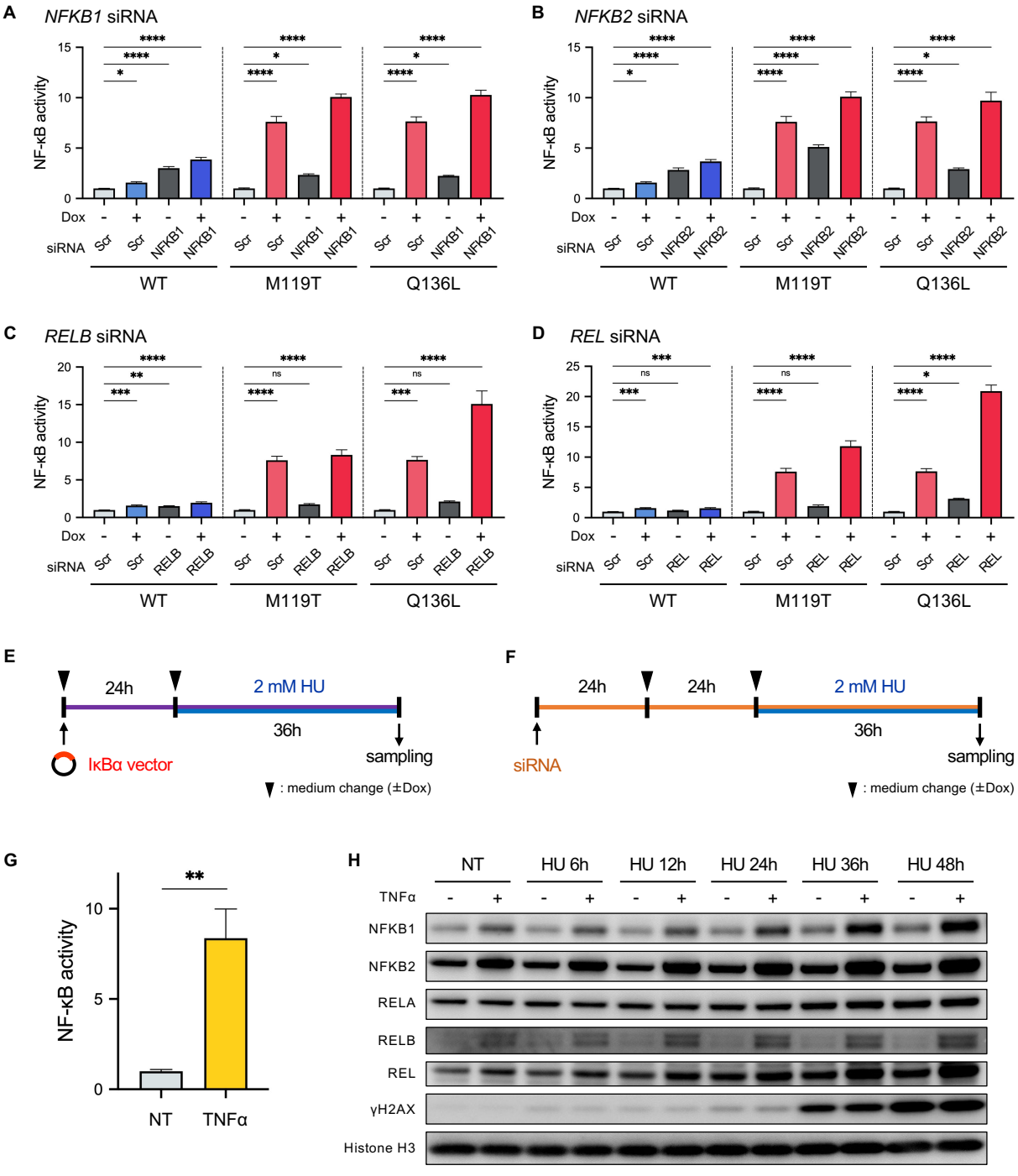
A
NFKB1 siRNA
B
NFKB2 siRNA
C
RELB siRNA
D
REL siRNA
NF-κB activity
Dox
siRNA
Scr
NFKB1
NFKB2
RELB
REL
WT
M119T
Q136L
E
24h
2 mM HU
36h
sampling
IκBα vector
: medium change (±Dox)
F
24h
24h
2 mM HU
36h
sampling
siRNA
: medium change (±Dox)
G
NF-κB activity
NT
TNFα
H
NT
HU 6h
HU 12h
HU 24h
HU 36h
HU 48h
TNFα
NFKB1
NFKB2
RELA
RELB
REL
γH2AX
Histone H3

Figure S7. Association between NF-κB signaling activity and the replication stress response

(A-D) NF-κB-dependent luciferase assay using CARD14-inducible cell lines to test the effect of depletion of NF-κB subunits, NFKB1 (A), NFKB2 (B), RELB (C), and REL (D); n = 5 independent experiments; error bars represent SEM. Statistical significance was calculated using ordinary one-way ANOVA with multiple comparisons test. **P* < 0.05, ***P* < 0.01, ****P* < 0.001, *****P* < 0.0001; ns, not significant. Scr, scramble (negative control).

(E and F) Schematic depicting timeline of cells treatment with 2 mM HU following IκBα overexpression (E) or RNA interference of NF-κB subunits (F).

(G) NF-κB-dependent luciferase assay performed using U2OS cells to test the NF-κB-activation potency of TNFα; n = 4 independent experiments; error bars represent SEM. Statistical significance was calculated using two-tailed *t*-test. ***P* < 0.01.

(H) Immunoblots showing the levels of DNA damage and the expression levels of NF-κB subunits following HU treatment, with or without TNFα stimulation. NT, non-treatment. WT, wild-type; M119T, p.Met119Thr; Q136L, p.Gln136Leu.

Figure S8

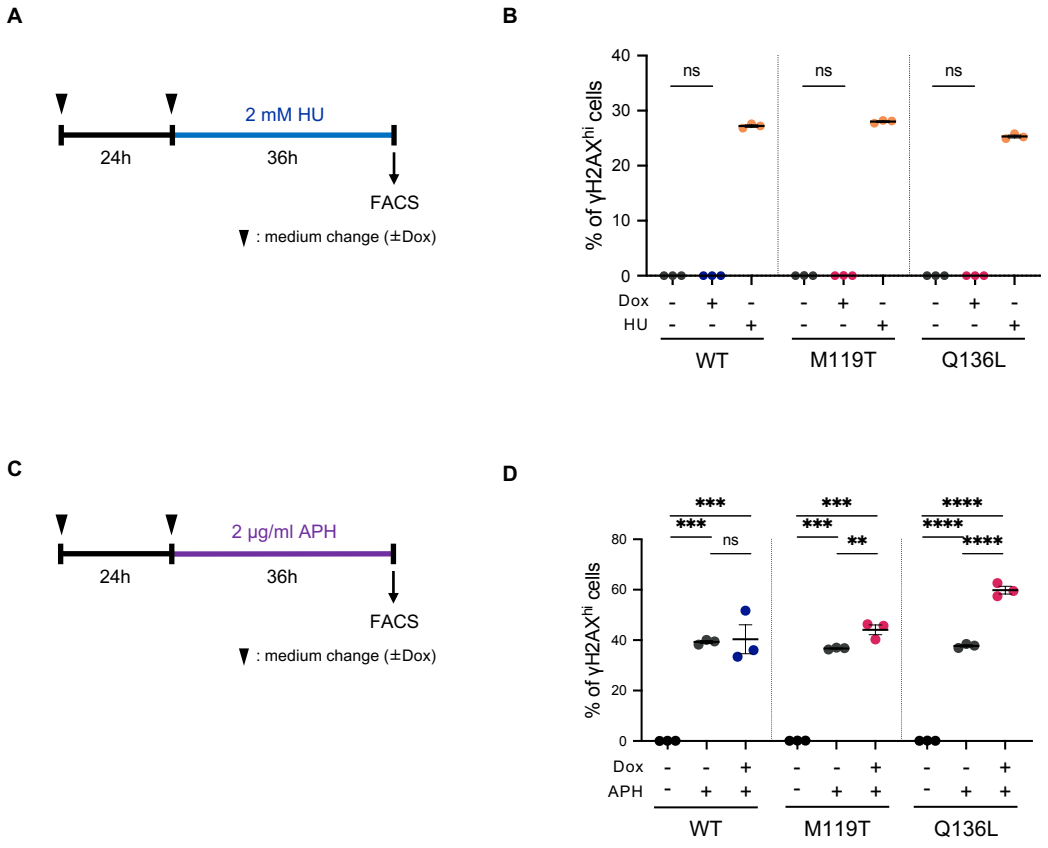
A
2 mM HU
24h
36h
FACS
▼ : medium change (±Dox)
B
% of γH2AX^hi cells
ns
Dox
HU
WT
M119T
Q136L
C
2 μg/ml APH
24h
36h
FACS
▼ : medium change (±Dox)
D
% of γH2AX^hi cells
***
ns
**
****
Dox
APH
WT
M119T
Q136L

Figure S8. FACS-based analyses for evaluating the replication stress response

(A) Schematic depicting timeline of when cells treated with HU for FACS analysis.

(B) CARD14 cell lines were incubated in the presence or absence of Dox for 36 h and harvested to estimate the levels of γH2AX by FACS. CARD14 expression per se did not increase the percentage of $\gamma H2AX^{hi}$ cells.

(C) Schematic depicting timeline of when cells were treated with APH for FACS analysis.

(D) A clear increase in the percentage of $\gamma H2AX^{hi}$ cells following APH treatment was observed in mut-CARD14 expressing cells. Statistical significance was calculated using one-way ANOVA with multiple comparisons test. $^{**}P < 0.01$, $^{***}P < 0.001$, $^{****}P < 0.0001$; ns, not significant. WT, wild-type; M119T, p.Met119Thr; Q136L, p.Gln136Leu.

Figure S9

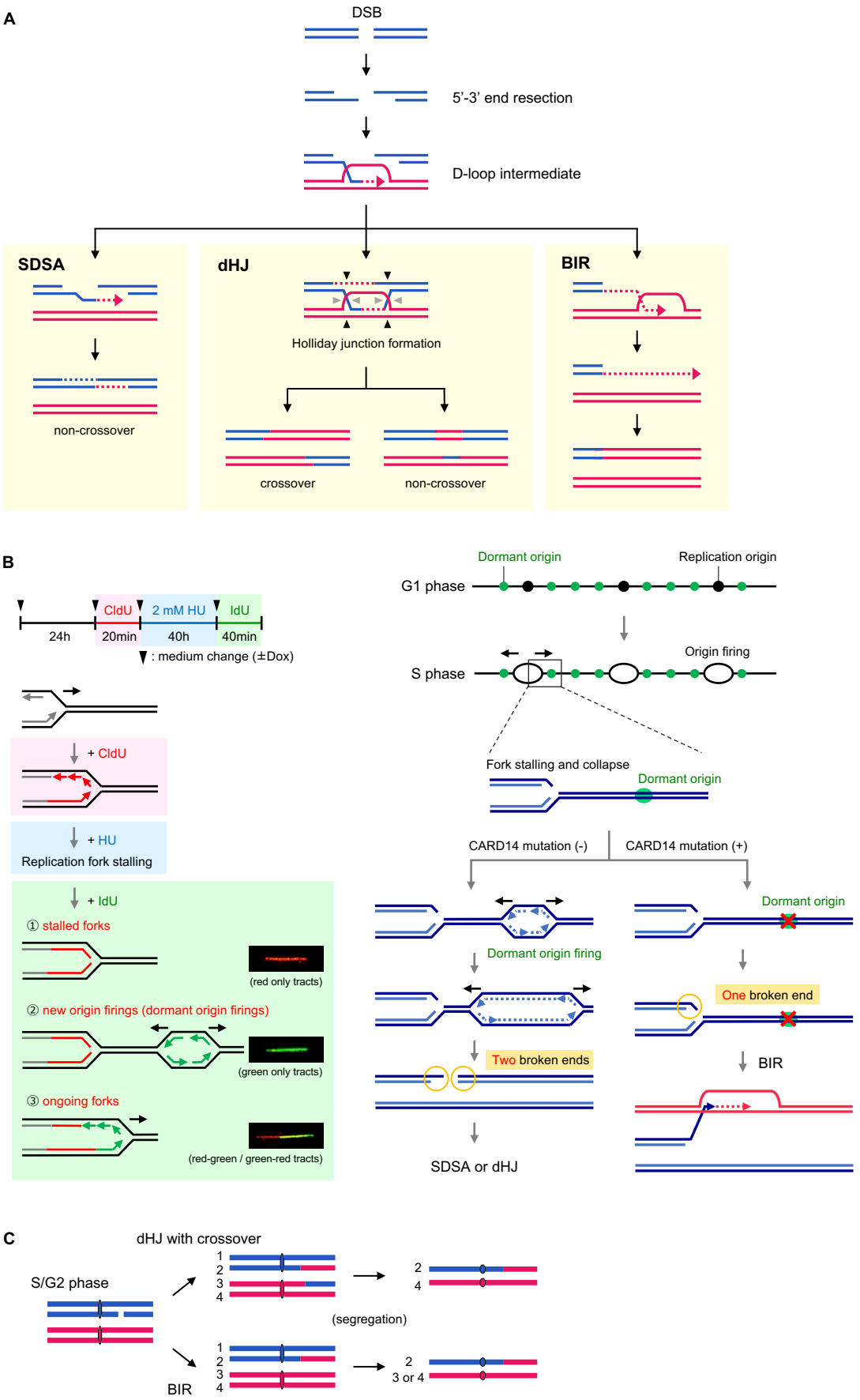
A
DSB
5'-3' end resection
D-loop intermediate
SDSA
non-crossover
dHJ
Holliday junction formation
crossover
non-crossover
BIR
B
CldU
2 mM HU
IdU
24h
20min
40h
40min
: medium change (±Dox)
+ CldU
+ HU
Replication fork stalling
+ IdU
① stalled forks
(red only tracts)
② new origin firings (dormant origin firings)
(green only tracts)
③ ongoing forks
(red-green / green-red tracts)
Dormant origin
Replication origin
G1 phase
Origin firing
S phase
Fork stalling and collapse
Dormant origin
CARD14 mutation (-)
CARD14 mutation (+)
Dormant origin
Dormant origin firing
One broken end
Two broken ends
BIR
SDSA or dHJ
C
dHJ with crossover
S/G2 phase
1
2
3
4
2
4
(segregation)
BIR
2
3 or 4

Figure S9. Three different HR pathways repairing collapsed forks

(A) HR initiates with a 5′-3′ end resection which produces a 3′ single-stranded end that invades a homologous template to form a displacement loop (D-loop) intermediate. All three sub-pathways can ensue from this D-loop structure and their outcomes are different. In SDSA, the nascent strand is displaced to anneal to the other 3′ single-stranded end, resulting in a non-crossover outcome. In the dHJ pathway, also referred to as DSB repair, the second DNA end is captured by the D-loop and a dHJ intermediate is formed. The following resolution can generate either a crossover (cleavage at black arrowheads on one side and gray arrowheads) or a non-crossover (cleavage at black or gray arrowheads) outcome. In BIR, extensive DNA synthesis from the invading end occurs when only one broken end is available for repair.

(B) Schematic showing the treatment of the cells, and representative images of three types of fibers are shown on the left. Suppression of dormant origin activation can cause the situation in which only one broken end is available for repair.

(C) Long-tract LOH observed in RM can be mediated by two HR pathways, BIR or dHJ, with a crossover outcome. LOH of entire distal regions of chromosomes may arise when DSBs are repaired by these two pathways in S/G2 phase and recombinant sister chromatids segregate to different daughter cells in the M phase.

Figure S10

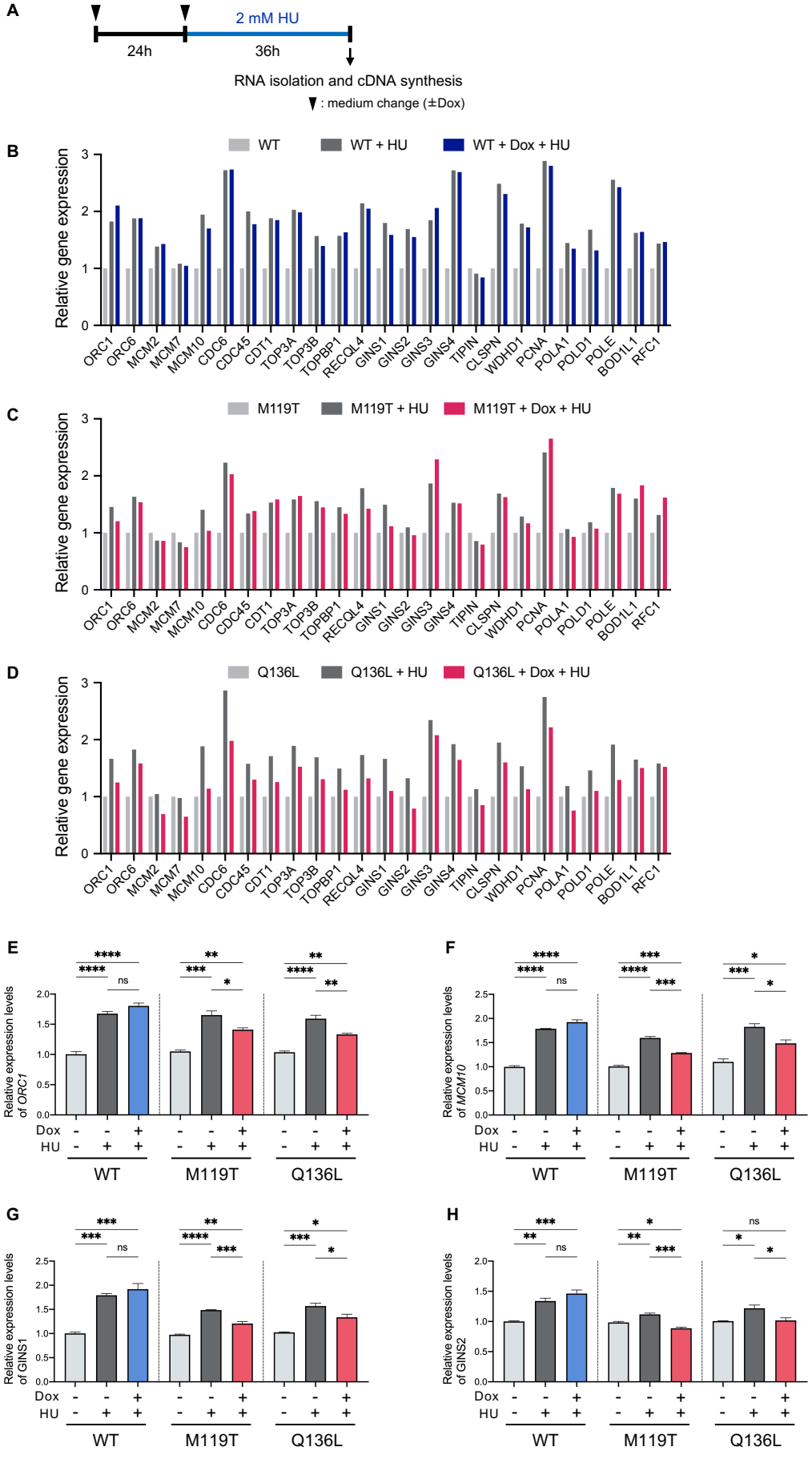
A
2 mM HU
24h
36h
RNA isolation and cDNA synthesis
: medium change (±Dox)
B
WT
WT + HU
WT + Dox + HU
Relative gene expression
ORC1 ORC6 MCM2 MCM7 MCM10 CDC6 CDC45 CDT1 TOP3A TOP3B TOPBP1 RECQL4 GINS1 GINS2 GINS3 GINS4 TIPIN CLSPN WDHD1 PCNA POLA1 POLD1 POLE BOD1L1 RFC1
C
M119T
M119T + HU
M119T + Dox + HU
Relative gene expression
ORC1 ORC6 MCM2 MCM7 MCM10 CDC6 CDC45 CDT1 TOP3A TOP3B TOPBP1 RECQL4 GINS1 GINS2 GINS3 GINS4 TIPIN CLSPN WDHD1 PCNA POLA1 POLD1 POLE BOD1L1 RFC1
D
Q136L
Q136L + HU
Q136L + Dox + HU
Relative gene expression
ORC1 ORC6 MCM2 MCM7 MCM10 CDC6 CDC45 CDT1 TOP3A TOP3B TOPBP1 RECQL4 GINS1 GINS2 GINS3 GINS4 TIPIN CLSPN WDHD1 PCNA POLA1 POLD1 POLE BOD1L1 RFC1
E
Relative expression levels of ORC1
Dox
HU
WT
M119T
Q136L
F
Relative expression levels of MCM10
Dox
HU
WT
M119T
Q136L
G
Relative expression levels of GINS1
Dox
HU
WT
M119T
Q136L
H
Relative expression levels of GINS2
Dox
HU
WT
M119T
Q136L

Figure S10. qPCR screening analysis of replication-related genes revealed the suppressive state of new origin firing in mutant CARD14 expressing cells

(A-D) RNA was isolated from CARD14 cell lines which were incubated in the presence or absence of Dox for 24 h and with or without 2 mM HU for 36 h (A). Gene expression levels were analyzed by qPCR (n =1 biological replicate, each with two technical replicates) (B-D). Note that expression values were normalized to ACTB expression. (E-H) Gene expression levels of *ORC1* (E), *MCM10* (F), *GINS1* (G), and *GINS2* (H) were further analyzed using the newly prepared samples; n = 3 independent experiments; error bars represent SEM; Statistical significance was calculated using one-way ANOVA with multiple comparisons test. **P* < 0.05, ***P* < 0.01, ****P* < 0.001, *****P* < 0.0001; ns, not significant. WT, wild-type; M119T, p.Met119Thr; Q136L, p.Gln136Leu.

Figure S11

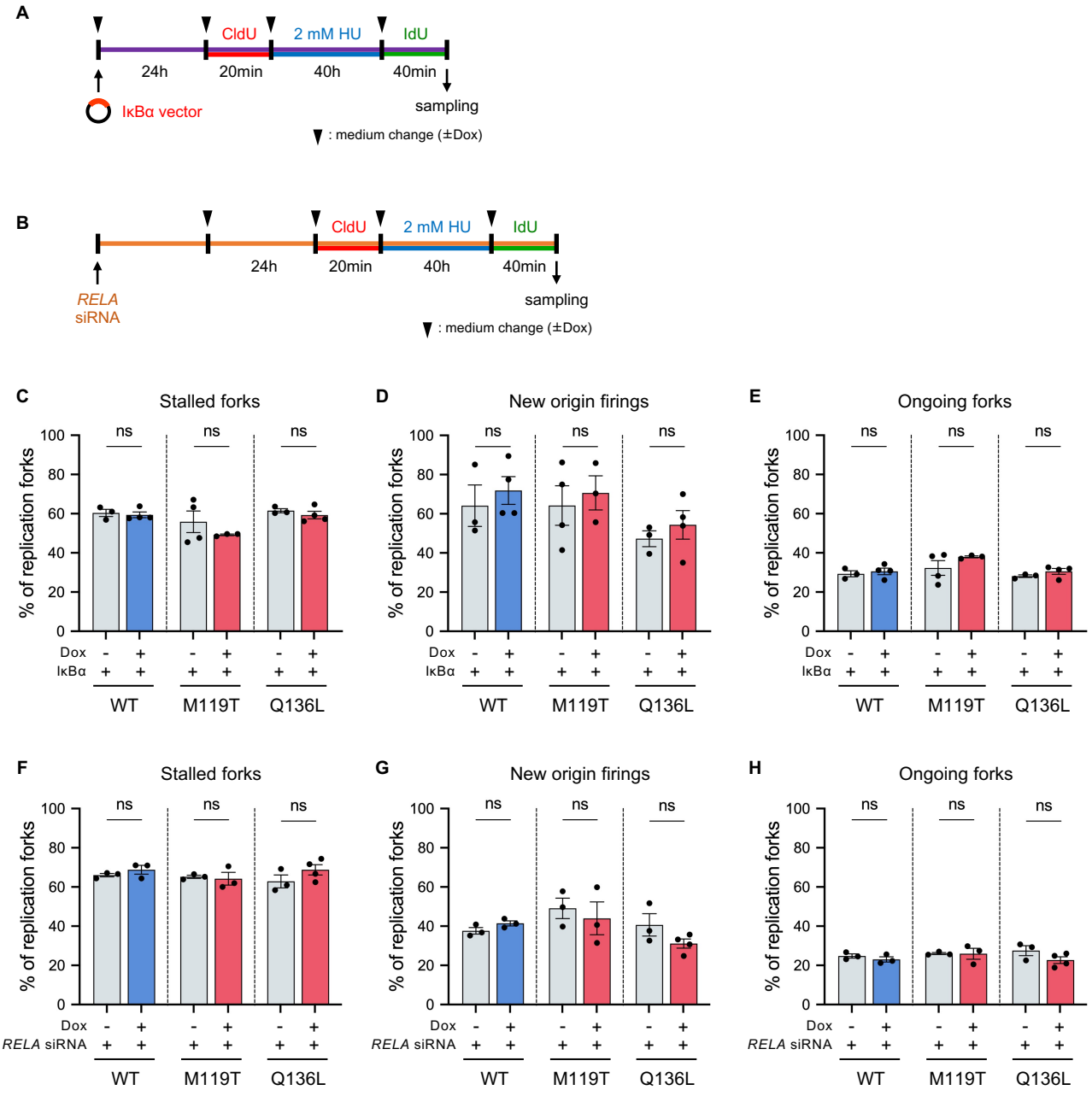
A
CldU
2 mM HU
IdU
24h
20min
40h
40min
sampling
IκBα vector
: medium change (±Dox)
B
CldU
2 mM HU
IdU
24h
20min
40h
40min
sampling
RELA siRNA
: medium change (±Dox)
C
Stalled forks
D
New origin firings
E
Ongoing forks
% of replication forks
ns
Dox
IκBα
WT
M119T
Q136L
F
Stalled forks
G
New origin firings
H
Ongoing forks
RELA siRNA

Figure S11. Alteration of DNA replication dynamics depending on the activity of the NF-κB signaling pathway

(A and B) Schematic depicting the timeline of cells labeling with CldU and IdU in the presence of HU treatment following IκBα overexpression (A) or RNA interference of RELA (B).

(C-H) Quantification of the percentage of stalled forks (C and F), new origin firings (D and G), and ongoing forks (E and H) to all CldU-labeled forks under the condition of IκBα overexpression (C-E) or RELA depletion (F-H); n = 3 independent experiments; error bars represent SEM. Statistical significance was calculated using the two-tailed t-test. ns, not significant. WT, wild-type; M119T, p.Met119Thr; Q136L, p.Gln136Leu.

Table S1

Gene	(MIM number, RefSeq)								
	Chromosome position	Nucleotide alteration	Amino acid alteration	Zygosity	dbSNP	Allele Frequency in Databases			
						1K Genomes	HGVD	GnomAD _Exome	GnomAD _Genome
ABCA12	(MIM 607800, NM_173076.3)								
	chr2: 215847009	c.4481T>C	p.Ile1494Thr	Heteroygous	rs1263698595	-	-	0.000004	0.00006
	chr2: 215876166	c.2329T>A	p.Ser777Thr	Homozygous	rs7560008	0.962906	0.9992	0.999503	0.99809
ALOX12B	(MIM 603741, NM_001139.3)								
	-	-	-	-	-	-	-	-	-
ALOXE3	(MIM 607206, NM_001165960.1)								
	chr17: 8022065	c.32C>T	p.Pro11Leu	Heteroygous	rs3027232	0.374	0.5816	0.334048	0.27294
CASP14	(MIM 605848, NM_012114.3)								
	-	-	-	-	-	-	-	-	-
CDSN	(MIM 602593, NM_001264.5)								
	chr6: 31083813	c.1579A>G	p.Asn527Asp	Homozygous	rs3130981	0.8337	0.8509	0.757978	0.76845
	chr6: 31084163	c.1229T>C	p.Leu410Ser	Homozygous	rs3132554	0.647	0.653	0.570698	0.56702
	chr6: 31084787	c.605T>C	p.Phe202Ser	Homozygous	rs707913	0.281	0.2985	0.232725	0.26226
	chr6: 31084964	c.428A>G	p.Asn143Ser	Homozygous	rs3130984	0.8345	0.8515	0.756159	0.76873
CERS3	(MIM 615276, NM_001290341.2)								
	-	-	-	-	-	-	-	-	-
CYP4F22	(MIM 611495, NM_173483.4)								
	-	-	-	-	-	-	-	-	-
FLG	(MIM 605776, NM_004467.4)								
	chr8: 17731961	c.314C>T	p.Pro105Leu	Heteroygous	rs2653406	0.154	0.1056	0.114235	0.13326
GJB3	(MIM 603324, NM_024009.3)								
	-	-	-	-	-	-	-	-	-
GJB4	(MIM 605425, NM_153212.3)								
	chr1: 35225395	c.-323+6G>A	N/A	Heteroygous	rs28433288	0.0823	0.072	-	0.04293
	chr1: 35227362	c.507C>G	p.Cys169Trp	Heteroygous	rs79193415	0.0313	0.0714	-	-
KRT1	(MIM 139350, NM_006121.4)								
	chr12: 53069014	c.1898A>G	p.Lys633Arg	Heteroygous	rs14024	0.2756	0.5973	0.309242	0.26635
KRT2	(MIM 600194, NM_000423.3)								
	chr12: 53045615	c.311_312insCGGCAGTGGCTTTGGAGG	p.Gly103_Phe108dup	Heteroygous	rs532019270	0.1807	0.6119	-	0.00019
	chr12: 53045626	c.301A>G	p.Ser101Gly	Heteroygous	rs2634041	0.3756	0.748	-	0.1137
KRT10	(MIM 148080, NM_000421.4)								
	chr17: 38975328	c.1459C>T	p.His487Tyr	Heteroygous	rs17855579	0.6971	0.4336	0.66284	0.74636
	chr17: 38978462	c.376G>A	p.Gly126Se	Heteroygous	rs77919366	0.1328	0.0355	0.193686	0.17672
	chr17: 38978536	c.302G>C	p.Ser101Thr	Homozygous	rs4261597	0.9992	1	0.998524	-
LIPN	(MIM 613924, NM_001102469.2)								
	chr10: 90530660	c.731C>A	p.Thr244Asn	Heteroygous	rs10788611	0.4451	0.5195	-	0.37522
LOR	(MIM 152445, NM_000427.3)								
	chr1: 153233991	c.574_585dup	p.Gly192_Gly195dup	Homozygous	rs11272549	0.6484	0.521	-	0.70116
NIPAL4	(MIM 609383, NM_001099287.1)								
	chr5: 156898690	c.637A>G	p.Arg213Gly	Heteroygous	rs6860507	0.5046	0.6544	0.496251	0.48558
PNPLA1	(MIM 612121, NM_001145717.1)								
	chr6: 36262153	c.691G>A	p.Ala231Thr	Homozygous	rs74946910	0.0401	0.1281	-	0.00819
POMP	(MIM 613386, NM_015932.6)								
	-	-	-	-	-	-	-	-	-
SDR9C7	(MIM 609769, NM_148897.3)								
	-	-	-	-	-	-	-	-	-
ST14	(MIM 606797, NM_021978.4)								
	-	-	-	-	-	-	-	-	-
SULT2B1	(MIM 604125, NM_177973.2)								
	-	-	-	-	-	-	-	-	-
TGM1	(MIM 190195, NM_000359.3)								
	-	-	-	-	-	-	-	-	-

Table S1. Genetic variations of individual 1 in the genes responsible for ichthyoses

Whole-exome sequencing showed that individual 1 has no pathogenic mutations in the listed genes, all of which are associated with non-syndromic ichthyoses. Genes related to syndromic ichthyoses were excluded from the list, because the patient had no extracutaneous symptoms.

Supplemental Material and Methods

Whole-exome sequencing

Whole-exome sequencing libraries were generated using the SureSelect Human All Exon V6 kit (Agilent Technologies), and enriched fragments were sequenced using the HiSeq 2500 platform (Illumina) with 100-bp paired-end reads to a median of 100× coverage. Cleaned fastq files were mapped onto the human reference genome version GRCh37 (hg19) using Burrows-Wheeler Aligner (BWA, v.0.7.10). SNVs, insertions, and deletions were called using the UnifiedGenotyper tool in the Genome Analysis Toolkit (GATK, v.1.6.13). Variants were analyzed using databases, such as the dbSNP (build 154), the 1000 Genomes Project (phase 3 release V3+), the Human Genetic Variation Database (HGVD, version 2.3), and the genome Aggregation Database (gnomAD, v2.1.1).